

Chapter 8

Laser Metal Deposition of Titanium Alloy and Titanium Alloy Composite: Case Studies

Abstract Laser metal deposition process, an additive manufacturing process offer lots of advantages such as ability to produce three dimensional (3D) object from the 3D computer aided design of the object- meaning that whatever can be drawn using any CAD software can be manufactured; the ability to make part with composite and functionally graded materials- because it can make use of multi materials at the same time; and the ability to build a new materials on an old material with good metallurgical integrity. These important characteristics of the laser metal deposition process have made it the manufacturing technology of the future. This chapter presents case studies on laser metal deposition of titanium alloy-Ti6Al4V and its composite materials because of the role this materials play in key industrial applications. Also, laser metal deposition process is a relatively new technology and some of the process physics are yet to be fully understood. These case studies shed more lights on the use of this additive manufacturing process for Ti6Al4V and its composites, the influence of some processing parameters on the evolving properties and how such processing parameters can be controlled in order to tailor the properties of the component being fabricated.

Keywords Additive manufacturing • Laser metal deposition • Material characterization • Ti6Al4V • Titanium alloy composite

8.1 Introduction

Titanium and its alloys are important materials in the aerospace, marine and petrochemical industries, to mention but few. The increase use of titanium and its alloys are base on the fact that, these materials have incredible properties that are required in a number of applications which include: excellent strength to weigh ratio, good corrosion resistance properties and these properties are often retained at elevated properties [1, 2]. In spite of these excellent properties of titanium and its

alloys, processing these materials pose a lot of challenges especially during machining. It results in a lot of tool failure because of the interaction between the tool material and titanium and its alloys [3–5]. To keep the cost of processing these materials low, there is need for an alternative manufacturing process with the capability to offset some of the problems enchanter while processing these materials. The ideal manufacturing process that is tool less and contactless is laser metal deposition process.

Laser metal deposition (LMD) process, an additive manufacturing technology, that uses the important properties of laser (see Chap. 2) as its energy source to process materials with the application of laser energy only to the needed area. Traditional manufacturing technology such as machining, involves material removal which is referred to as subtractive manufacturing process, differs from laser metal deposition process which is an additive manufacturing process. Laser metal deposition process fabricates three dimensional (3D) parts by using the information generated by the 3D computer aided design (CAD) data to build the part by adding materials layer by layer [6, 7]. This mode of manufacturing is unique because it does not generate waste materials such as chips that become problematic to manage during the manufacturing of some materials using the subtractive manufacturing process. Managing and disposing such chips could be too expensive while machining difficult to machine materials such as titanium and its alloys. With the laser metal deposition process, there is no such problem; this is because materials are added up in order to fabricate materials and with proper process parameters control, material usage efficiency—that is the ratio of materials actually used up during the deposition process and the actual material being delivered during the process, can be very high [8–11]. The un-used materials can also be re-used making the process waste free.

Processing parameters such as laser power, scanning velocity, powder flow rate and gas flow rate (see detail about each of these parameters in Chap. 4) play important roles in the evolution of properties in materials produced using the laser metal deposition process as well as the economy of the process [8, 12–17]. Case studies of laser metal deposition of Ti6Al4V and Ti6Al4V/TiC composites are presented in this chapter and some of the influences of these processing parameters on the properties of the laser metal deposited materials are analyzed. Scanning speed is an important process parameter in the laser metal deposition process and it also determines the speed of the manufacturing process. Scanning speed has a number of influence on the physical, metallurgical as well as the mechanical properties of the deposited materials. A case study on the influence of scanning speed on the properties of laser metal deposited Ti6Al4V is presented in the next section.

8.2 Case Study 1: Scanning Velocity Effect on Properties of Titanium Alloy Produced by Laser Metal Deposition Process

Ti6Al4V is an important material that is used in a number of industries including the automobile and aerospace industries because of its exciting properties. The major problem with titanium and its alloys is that, it poses a lot of challenges processing this material especially with machining processes. For this reason, it is very expensive to process because of a number of down time that is required to change the cutting tools and also the high cost of the cutting tool. The quest for alternative manufacturing process for difficult to machine materials lead to the use of additive manufacturing process which is a tool-less manufacturing method. Laser metal deposition process, an additive manufacturing technology, is an important manufacturing process that offers lots of advantages for producing three dimensional part as well as for repair of damaged parts. Laser metal deposition process is very sensitive to the processing parameters and it is capable improving the properties of materials. Fabricating moving parts for the aerospace, for example, will help to reduce the overall weight of the aircraft and also improve the fuel efficiency and hence help to reduce the carbon foot print of the aerospace industry. In this case study, the influence of scanning speed on the metallurgical and mechanical properties of laser metal deposited was investigated. Nd: YAG laser was used to deposit Ti6Al4V powder on Ti6Al4V substrate. The scanning velocity was varied between 0.005 and 0.095 m/s. The microstructures and microhardness of the samples were studied using the optical microscope Vickers hardness tester.

8.2.1 Introduction

Titanium and its alloys have a good combination of properties which include good corrosion resistance, high strength to weight ratio and the ability to retain these properties at elevated temperatures [18]. Titanium and its alloy find their applications in a number of industries because of these important properties. Ti6Al4V is an important titanium alloy with unique combination properties and structurally efficient for the fabrication of critical, high-performance parts which include automobile engine part, jet engine parts and airframe components [19]. However, titanium and its alloys are characterized as difficult to machine materials because of their chemical properties that make them be attracted to any material they come in contact with. This is why they react with cutting tool material causing damage to the cutting tool during machining operation. This has make machining titanium and its alloy very expensive to machine [3–5]. There is one of the reasons why there is need for an alternative manufacturing process for difficult to machine materials.

Laser Metal Deposition process is an important additive manufacturing technology which is a perfect alternative manufacturing process for processing titanium and its alloys because it is a contact-less manufacturing process [6]. Laser metal deposition process can be used to fabricate 3D parts directly from the 3D CAD image of the part no matter the complexity and it can be used to achieve repair of high valued component parts. Complex part can be made using the LMD process as a single unit part which helps in reducing the overall weight of such part thereby eliminating the weight of the extra materials used in joining process. This weight saving results in fuel savings for the transportation industries. Customized parts can be produced using this, manufacturing process at near mass production rate and with high material efficiency as well as help to improve buy-to-fly ratio of aircraft [20, 21]. High valued parts that were not repairable in the past can now be repaired using the LMD process because of low heat affected zone associated with the process [22, 23]. A lot of research has been reported in the academic literature about the relationship of the processing parameters and the properties of Ti6Al4V produced with the LMD process [13–17, 24]. It has been shown in the literature that LMD process is a highly un-linear process in relation to the process parameters. This case study according to Mahamood and Akinlabi [24], sought to understand the behaviour of the LMD process with respect to variation of scanning speed. The influence of the scanning speed on the resulting microstructure and the micro-hardness are presented.

8.2.2 Experimental Procedure

Ti6Al4V powder, Ti6Al4V substrate, 4.0 kW Nd-YAG laser, argon gas, and improvised glove box are the materials that were used in this experiment. The Ti6Al4V substrate and the Ti6Al4V powder used in this experiment are of 99.6% purity. The Ti6Al4V powder is of particle size range of 150–250 μm . The substrate was sand blasted and cleaned with acetone prior to the deposition process. The laser metal deposition process was achieved with the experimental set-up shown in Fig. 8.1a which is available at the National Laser Center, in council for scientific and industrial research (CSIR), Pretoria South Africa. The set-up consists of a kuka robot carrying a 4.0 kW Nd-YAG laser with coaxial powder nozzles. The spot size of the laser was maintained at 2 mm and the focal length was maintained at a distance of 195 mm above the substrate throughout the experiments. The powder was delivered through the argon gas medium at a constant flow rate of 4 l/min. A glove box shown in the set-up was improvised and filled with argon gas to protect the deposited samples from the attack of oxygen and nitrogen. The laser beam create a melt-pool on the surface of the substrate while the Ti6Al4V powder was delivered onto the melt-pool through the coaxial powder nozzles. The laser left on its path a solid track of the Ti6Al4V as it moves along the substrate. The laser power and the powder flow rate were kept constant at 3.5 kW and 2 rpm. The scanning speed was varied between 0.005 and 0.095 m/s as presented in Table 8.1.

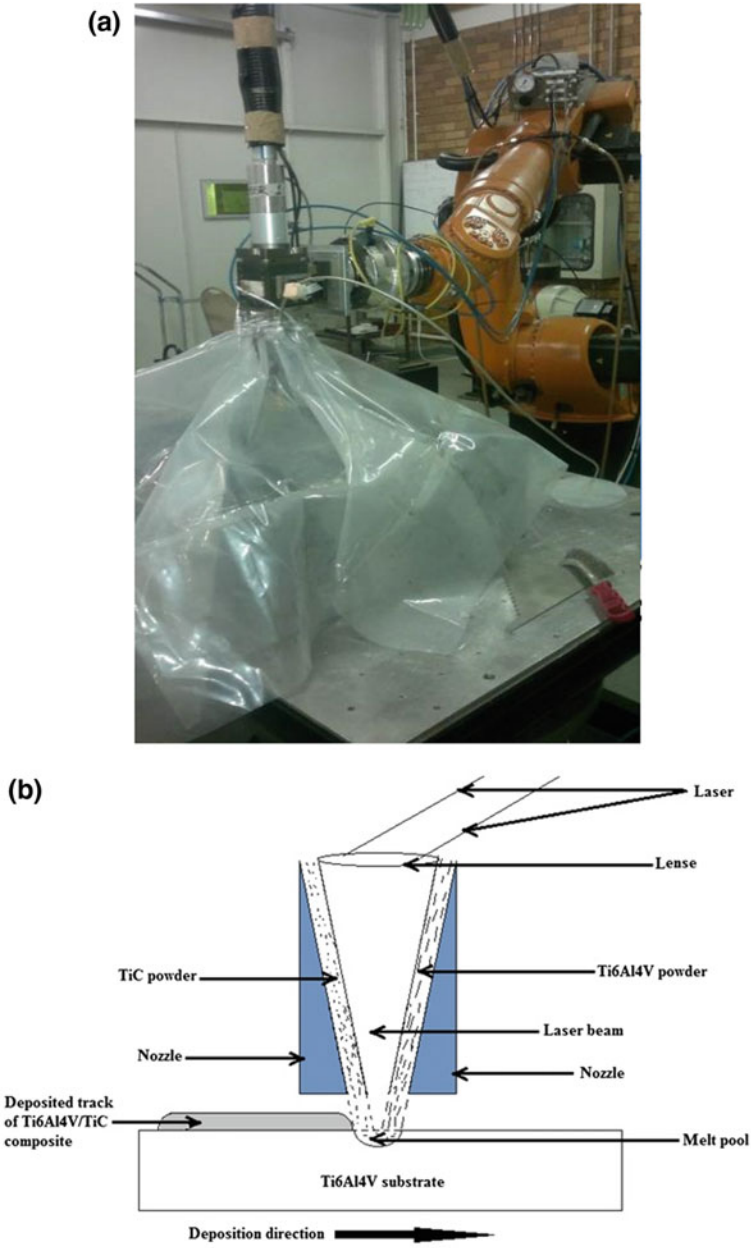


Fig. 8.1 a Pictorial diagram of the experimental set-up b Schematic of the LMD process [25]

Table 8.1 Experimental matrix

Sample designation	Scanning speed (m/s)
A	0.005
B	0.015
C	0.025
D	0.035
E	0.045
F	0.055
G	0.065
H	0.075
I	0.085
J	0.095

The experimental set-up and the schematic of the LMD process are shown in Fig. 8.1a, b respectively.

After the deposition process, the samples were cut across the deposition direction to reveal the cross section of the deposited samples.

The cut samples were mounted in hot resin, ground and polished following the standard metallurgical sample preparation for titanium and its alloys [21]. The microstructural samples were etched with Kroll reagent. Kroll's reagent consists of 100 ml of water with 3 ml of hydrofluoric acid and 4 ml of nitric acid. The etched samples were observed under Olympus BX51M Optical Microscopy (OP) that was equipped with an Olympus DP25 digital camera. The microhardness was measured using the Metkon Vickers hardness tester with a load of 500 g, dwelling time of 15 s distance between indentations kept at 15 μm following the ASTM standard [26].

8.2.3 Results and Discussion

The micrograph of the Ti6Al4V powder and substrate are shown in Fig. 8.2a and b respectively. The Ti6Al4V substrate is made up of alpha and beta grains that is typical of any Ti6Al4V. The alpha phase is shown as the lighter parts of the microstructure while the darker parts are the beta grain structure. The Ti6Al4V powder is spherically shaped because it is gas atomized. The microstructures of the samples deposited at 0.005 m/s and 0.055 m/s are shown in Fig. 8.3a and b respectively. The microstructure showed globular grains in the heat affected area. The globular grains are produced as a result of grain growth from the transmitted heat to this area from the melt-pool. The microstructure in the deposited zone is characterized by columnar grains which grow epitaxially on the globular grains as

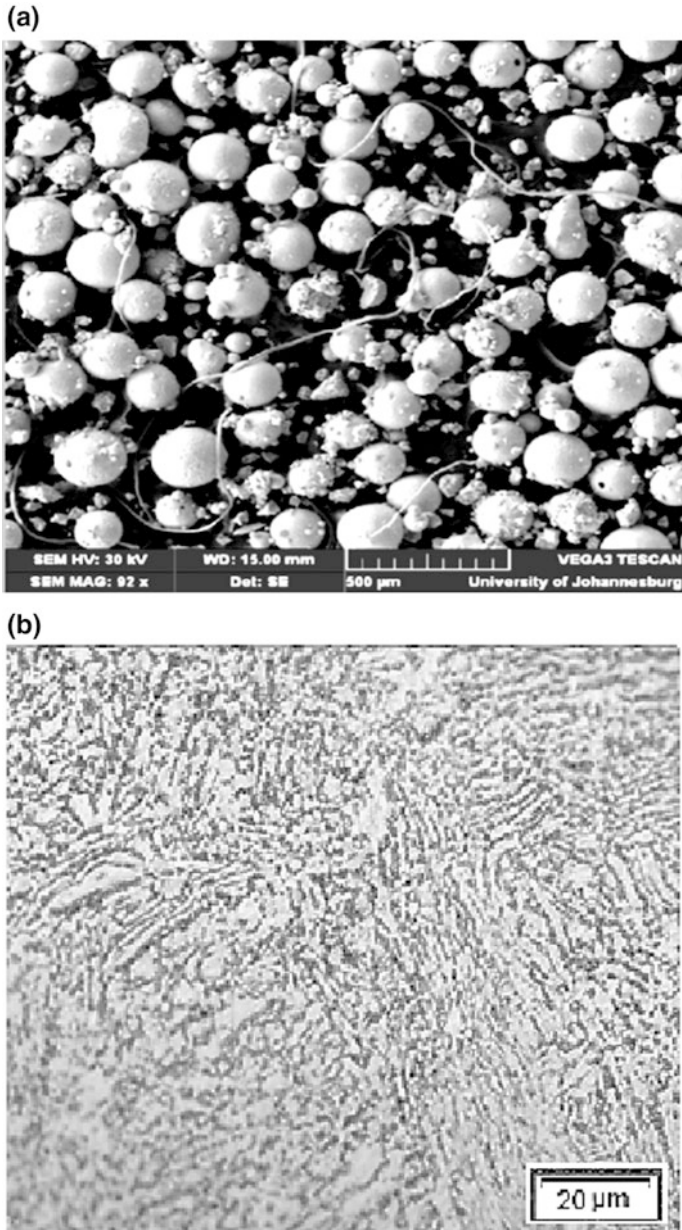


Fig. 8.2 a SEM micrograph of the Ti6Al4V. b Micrograph of the Ti6Al4V substrate

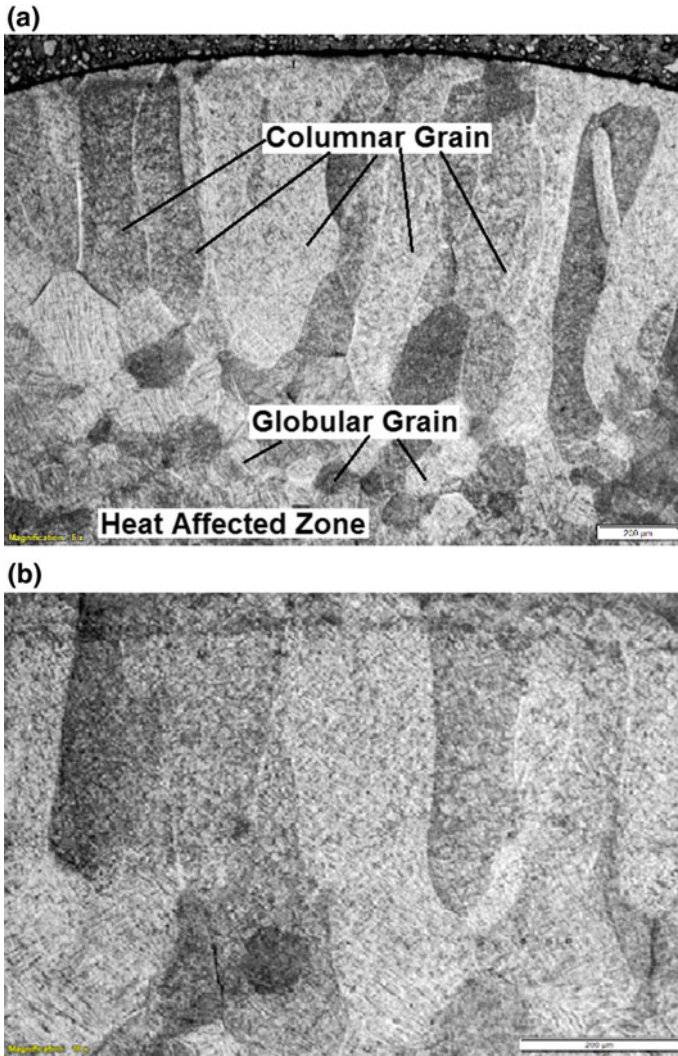


Fig. 8.3 Micrograph of the sample at the scanning speed of **a** 0.005 m/s and **b** 0.055 m/s

shown in Fig. 8.3a. The directional solidification of the melt-pool is responsible for the columnar grains. The substrate is cold and it act as heat sink that causes the columnar grains to be formed. The quantity of these globular grains was found to increase as the scanning speed was increasing. At higher scanning speed, the columnar grains are smaller in size as compared to those at the lower scanning speed as shown in Fig. 8.3b. This is because, the laser material interaction time is

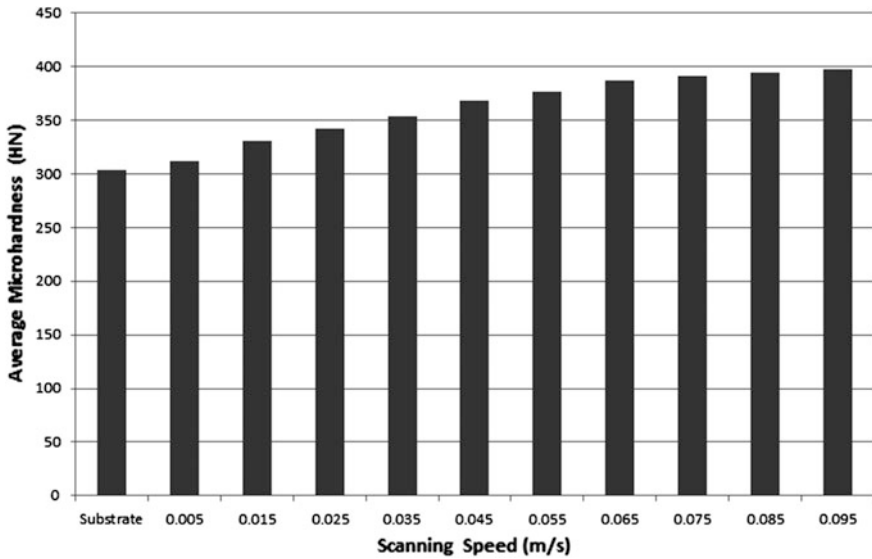


Fig. 8.4 Bar chart of the average Microhardness versus the scanning speed

longer at lower scanning speed that resulted in larger melt-pool formed. Larger melt-pool will result in the formation of larger globular grains that in turn form the larger columnar grains which are fewer in number at lower scanning speed.

On the other hand, at higher scanning speed, smaller melt-pool are created which solidified much quickly and hence causing little grain growth. This was why the globular grains formed at this higher scanning speed to be smaller and hence smaller and larger quantity of columnar grains formed. Since the columnar grains grow epitaxially on the globular grains, hence the columnar grain have direct relationship to the globular grains as shown in Fig. 8.3a and b.

The results of the microhardness is shown in the bar chart presented in Fig. 8.4. The microhardness was found to increase as the scanning speed was increasing. At lower scanning speed, the solidification rate was slower which helps to promote the formation of the Widmanstatten alpha as shown in Fig. 8.5a and hence the lower microhardness at lower scanning speed. At higher scanning speed, on the other hand, the melt-pool formed is smaller and the solidification is more rapid that promotes the formation of the martensitic alpha as seen in the microstructure shown in Fig. 8.5b.

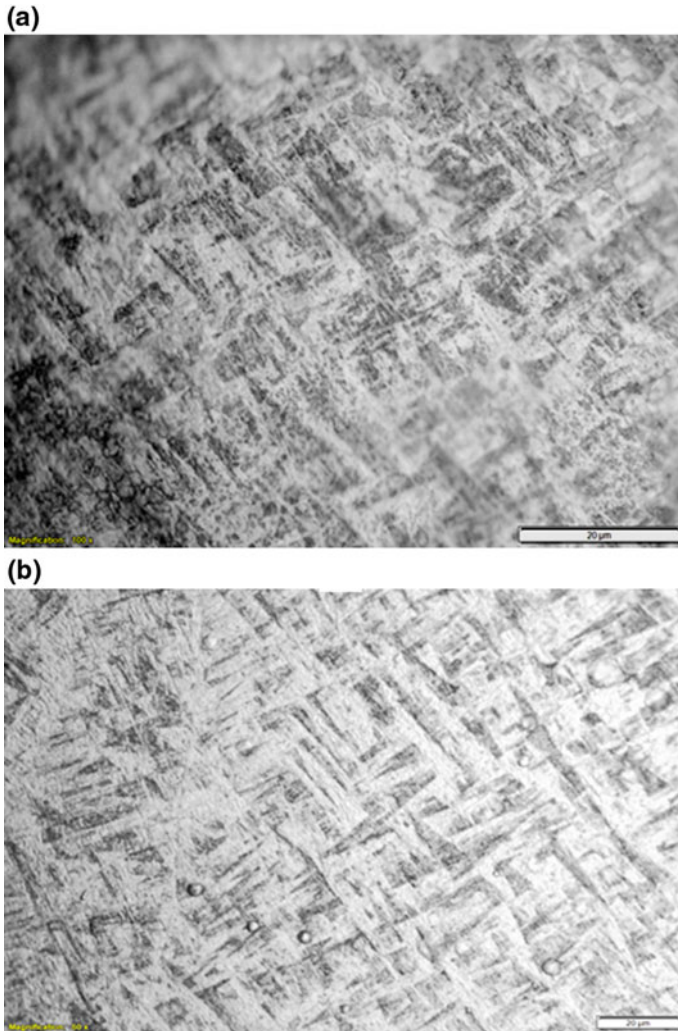


Fig. 8.5 Microstructure of sample at produced at scanning speed of **a** 0.025 m/s **b** 0.55 m/s

8.2.4 Conclusion

The excellent properties of the Ti6Al4V makes its application area to be on the rise. Repair of components that are made of Ti6Al4V will be required from time to time, therefore the laser metal deposition process, an important additive manufacturing technology will be needed in keeping these components in service for longer period of time. The influence of scanning speed on properties of laser deposited Ti6Al4V has been studied. The microstructure was found to change from Widmanstätten

structure at lower scanning speed to martensitic structure at higher scanning speed. Also, the microhardness was found to increase as the scanning speed was increased. The average microhardness of all the samples were found to be higher than that of the substrate because of the relatively high solidification rate that is associated with the LMD process. In order to control the hardness property of the deposited parts, the scanning speed can be effectively controlled. The next case study is on the influence of processing parameters on properties of laser metal deposited Ti6Al4V/TiC composite.

8.3 Case Study 2: Effect of Laser Power on Laser Metal Deposited Ti6Al4V/TiC Composite

The flexibility offered by laser metal deposition process, ability to make use of different materials such as metals and ceramics, makes it possible to deposit metal matrix composite material. The use of laser metal deposition process for the production of composite materials results in properties that are phenomena because; the process is characterized by rapid solidification of the melt pool that helped to produce microstructures that could not be produced through other process. The thermodynamic limitation does not also affect composite materials processed using the LMD process because of the rapid solidification in the process. The process parameters of laser metal deposition process also have a great influence on properties of deposited composite materials. In this section, the effects of laser power on the laser deposited titanium alloy composite of Ti6Al4V/TiC are analyzed.

8.3.1 Introduction

Ti6Al4V is the most widely used titanium alloy in the industry and it is often referred to as the workhorse in the industry because of its excellent properties [27–29]. It has the highest strength to weight ratio of any known material and it has very good corrosion resistance properties. Despite all these excellent properties, Titanium is difficult to machine and its wear resistance property is poor [3, 4, 30]. The reason for the poor wear resistance behaviour of Ti6Al4V is that it reacts with any material it comes in contact with, which is responsible for its been difficult to machine. When this material is involved in the rubbing action with another material, it generates a high temperature. This is what leads to galling of the Titanium to the cutting tool material during machining operation that results to tool failure.

8.3.2 *Wear Performance Behaviour of Ti6Al4V*

The wear resistance behaviour of Ti6Al4V is poor and it has a very high coefficient of friction [31]. The reason for the poor wear resistance behaviour of Titanium has been attributed to the low thermal conductivity and the low strain hardenability of this material [32]. The high chemical reactivity of Ti6Al4V causes a strong adhesion with itself, or with other materials that it comes in contact with [33]. During the rubbing action of Ti6Al4V and material, they tend to adhere to the surface of the other material that results in very high friction. This high frictional forces cause lots of heat to be generated during the rubbing action. The heat generated finds it difficult to escape out of the two surfaces because of the poor thermal conductivity of Ti6Al4V that then result in wear of the surfaces. That is why Ti6Al4V needs surface modification if this material will be used in application requiring rubbing action.

A number of surface modifications have been reported in the literature to improve the wear-resistance behaviour of Ti6Al4V. Hard wear resistance metal matrix composite materials are often deposited on the surface of Ti6Al4V using laser metal deposition process in the literature in order to improve its wear-resistance performance [34–37].

Metal Matrix Composites (MMCs) materials are engineering material, developed in order to improve the material's properties [38]. MMCs have better properties compared to other alloyed materials such as higher wear and fatigue resistance, higher deformation resistance, higher rigidity and better thermal shock resistance. It has been proved that the tribological properties of titanium alloys can be improved by reinforcing them with ceramics [39]. Titanium Metal Matrix Composite (TiMMC) is an important engineering material with excellent combination of properties that is used in applications such as the production of connecting rods and piston pins which gives a better fuel economy, reduced emissions, lower noise and vibration as a result of the weight reduction it provided [40]. Forming metal matrix composite reinforced with ceramic coating on the surface of Ti6Al4V has been proved to be very effective in improving the wear resistance behaviour of this important aerospace alloy. Wang et al. [41], investigated the effect of Titanium Carbide (TiC) volume fraction on the wear behaviour of Ti6Al4V/TiC composite. The composite for different volume fractions of the Ti6Al4V/TiC with 8, 15, 24 and 74 vol% TiC composites were produced at constant processing parameters. They found out that the wear resistance was not improved when the vol.% TiC was less than 15 vol% TiC. As the TiC volume fraction was increased beyond 15 vol% TiC, the wear resistance performance was increased.

Different ceramics has been used to reinforce Titanium and its alloy as MMC in the literature. Kim et al. [42] reinforced Ti6Al4V powder with Titanium carbide (TiC) to produce composites using powder metallurgy process. The TiC was developed using a gas–solid in situ reaction process. Titanium Carbide, Aluminum Carbide and Vanadium Carbide were produced during the chemical reactions. Of all the carbides formed during the chemical reactions, only Titanium Carbide was left

after the sintering. The TiC/ Ti6Al4V composite formed showed higher hardness, higher elastic modulus, higher tensile strength, and better wear resistance than wrought Ti–6Al–4V alloys. Cui et al. [43] used a 2 kW Nd: YAG laser to synthesize Ti/TiN metal matrix composite coating to modify the surface of pure Titanium. The Ti/TiN metal matrix composite coating had higher hardness and better wear resistance, Joshi et al. [44] used mechanical activation process of reactive milling to produce Ti–TiO₂ composite powders from titanium powders. The microhardness was shown to increase with increasing milling time. Alman and Selamat et al. [45] also produced SiC/Ti6Al4V composite to modify the surface structure of a Ti6Al4V alloy using laser processing. Lapin et al. [46] studied the effect of various volume fractions of Al₂O₃ particles on property of Ti6Al4V. The yield stress was found to be increased with increasing volume fraction of Al₂O₃ particles. De Castro et al. [47] used arc-melting technique to produce Y₂O₃-dispersed titanium with Y₂O₃ (Zr₂O₃, R₂O₃ (R means rare element)) content ranging between 0.3 and 0.7 wt% was starting from Ti and Y₂O₃. A uniform nano-dispersion of Y₂O₃ particles were found in all the alloys. The Y₂O₃ nano-dispersion effectively strengthened these materials. Zhanga et al. [48] produced Ti6Al4V/TiC, Ti6Al4V/TiB and Ti6Al4V/TiC+ TiB by an in situ method. The microhardness was found to be improved with the TiC, TiB and the TiC+ TiB reinforcements and the microhardness does not really depend on the morphology of reinforcements.

The matrix alloy and the reinforcement material should be chosen based on their chemical compatibility and the ability of the matrix to wet the reinforcement [49]. TiC possesses desirable combination of properties that include: high hardness, high melting point, and excellent thermal and chemical stability making them to be useful in many wear resistance applications [50]. TiC particles are more compatible with Titanium and its alloy [51]. TiC has higher wetting and higher interfacial bonding with the matrix material [52]. It has been proved to be very stable thermodynamically in Ti6Al4V and bonds very well with the matrix [53]. Because TiC is thermodynamically stable in Ti6Al4V, the particle matrix interface that results is very stable [51]. This important property is absent in some other carbides like Silicon Carbide (SiC) because, there is chemical interactions between the SiC and Titanium which results in an unstable particle-matrix interface [53]. Other areas of application of Titanium MMC include: Aero engine compressor blades, combustion chamber, Throat, exit nozzle, engine valves and fins thrust, aero engines for compressor blades due to its higher elevated temperature resistance property [29, 54, 55].

A number of researches on the laser metal deposition of Ti6Al4V/TiC composite have also been reported in the literature [56–58]. Obiolodan and Strucker [59] used the LMD process to produce composites of 10 and 5wt%TiC/Ti6Al4V on Ti6Al4V substrate. Popoola et al. [35] studied alloys of TiC/Ti6Al4V composite at various TiC compositions. Wang et al. [41] also deposited TiC/Ti6Al4V composite at different TiC compositions. Ochonogor et al. [60] studied the effect of the TiC ratio on the wear resistance performance of Ti/TiC composite, using laser metal

deposition. In this case study, the influence of laser power on the properties of laser metal deposited Ti6Al4V/TiC composite is analyzed.

8.3.3 Experimental Method

The substrate material used was in this case study is Ti6Al4V alloy in annealed form. It was supplied by VSMPO-AVISMA Corporation in Russia. This alloy is 99.6% pure; and it contains approximately 6 w% of Aluminum, which is an alpha-stabilizing element and approximately 4 w% of Vanadium, a beta-phase stabilizing element. The chemical composition of the substrate material is presented in Table 8.2

The substrates were cut into a rectangular shape, with dimensions of 72 mm \times 72 mm \times 5 mm. The substrate were sandblasted and cleaned with acetone before the deposition process. The purpose of sandblasting the substrate was to aid the laser-power absorption process, because a shining surface would reflect most of the laser beam. The powders used were Ti6Al4V and TiC powders. The particle size of the Ti6Al4V powder is between 120 and 350 μ m. It is a spherically shaped gas-atomized powder. The TiC powder is of particle size range below 60 μ m. The Ti6Al4V powder was supplied by F.J. Brodmann and Co., L.L.C., Louisiana. The detail of the material composition is given in Table 8.3. Atomized powders have a spherical shape and smooth surfaces. They exhibit low surface oxidation because of the reduced total surface area. The TiC powder used in this research is ball-milled powder, also supplied by F.J. Brodmann and Co., L.L.C., Louisiana. It has an irregular shape, which is characteristic of a ball-milled powder. The chemical composition of the TiC powder is presented in Table 8.4.

The laser metal deposition experimental set-up is the one shown in Fig. 8.1. The deposition was achieved by a Kuka robot carrying the laser head and coaxial powder nozzles. The substrate is fixed on the laser bed; while the robot moves the

Table 8.2 Chemical composition of Ti6Al4V substrate

Element	Al	V	Fe	C	N ₂	H ₂	O ₂	Ti
W%	6.42	3.91	0.19	0.008	0.006	0.004	0.155	Balance

Table 8.3 Chemical composition of the Ti6Al4V powder

Element	Al	V	Fe	C	N ₂	H ₂	O ₂	Ti
W%	6.20	3.90	0.18	0.008	0.005	0.005	0.150	Balance

Table 8.4 Chemical composition of the TiC powder

Element	C	O ₂	N ₂	Fe	Al	Na	Ti
%	19.5	0.28	0.4	0.045	0.03	0.026	Balance

laser, in order to achieve the deposition process. The various elements of the experimental set-up are described below. The laser used in this study was Nd: YAG laser with a wavelength of $1.06\ \mu\text{m}$ and maximum power of 4.0 kW. The laser head was fixed on the end effector of the robot. The beam diameter was maintained at approximately 2 mm at a focal distance of 195 mm above the substrate. A glove box shown in Fig. 8.1 was improvised to prevent the deposited parts from environmental attack, such as Nitrogen and Oxygen. A transparent flexible plastic sheet was wrapped around the end effector in such a way that when the robot reached for the deposition process, the flexible plastic wrapping covers the box on the laser bed and the shielding gas was run to cover the deposit, and to protect it from the atmosphere, and to prevent oxidation. The powder feeder used in this study consists of two hoppers, as shown in Fig. 8.6. The two hoppers allow for the deposition of two powders simultaneously.

The nozzles from the hoppers were attached coaxially to the end-effector of the Kuka robot. The powders are protected by Argon gas. The hopper is calibrated in revolutions per minute (rpm). The two powders used in this study were placed separately in each hopper. Putting the powders in separate hoppers and delivering the powders simultaneously is more advantageous than premixing the powders. The problem of segregation is eliminated as a result of a density difference in the powders that were pre-mixed.



Fig. 8.6 Powder feeder

Table 8.5 Processing Parameters

S/N	Laser power (kW)	Scanning speed (m/s)	Powder flow rate (g/min)	Gas flow rate (l/min)
1	1	0.05	4	2
2	1.5	0.05	4	2
3	2.0	0.05	4	2
4	2.5	0.05	4	2
5	3.0	0.05	4	2

The laser power was varied between 1 kW and 3 kW; the remaining processing parameters were kept at fixed values in order to establish the influence of only the laser power. The processing parameters that are used in this study are presented in Table 8.5.

The laser metal deposition process was achieved by the robot moving the laser head towards the substrate, which was fixed inside the glove box. The laser heats up the surface of the substrate and creates a melt pool on the substrate. The powders are delivered into the melt pool through the coaxial nozzles, which were attached to the end-effector of the robot. As the melt pool solidifies, it forms a track of the deposited materials on the substrate. The photograph of the deposit is shown in Fig. 8.7. The deposit was allowed to cool before being removed from the glove box, because the Titanium could still react with the atmospheric oxygen if the deposit is hot and exposed to the atmosphere. After the deposition process was completed.

The surface roughness of the deposit and the wear track of the samples were measured with the stylus surface analyzer by Jenoptik, equipped with Hommelmap

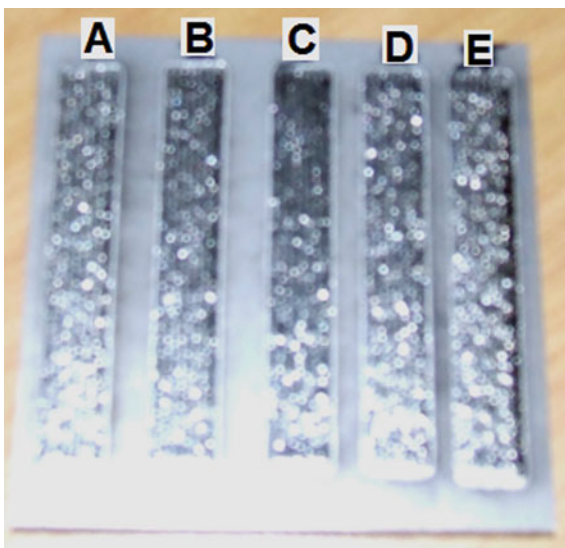
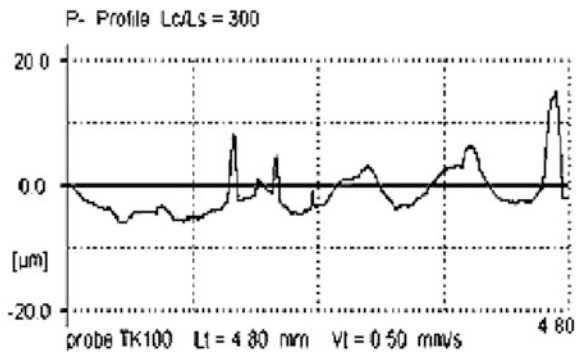
Fig. 8.7 Pictorial diagram of deposited samples



Fig. 8.8 Jenoptik surface profiler

Fig. 8.9 Surface profile of a deposited track with average roughness value of $1.0 \mu\text{m}$ [25]



6.2 software available at University of Johannesburg. The surface analyzer is shown in Fig. 8.8. The effective measuring length was 4.8 mm; the cut-off length was 0.8 mm; and the measuring range was $400 \mu\text{m}$. A sliding speed of 0.50 mm/s was selected; five measurements were taken on each of the samples, and the arithmetic average of the 2D roughness profiles (Ra) was recorded for each sample of interest. The measuring condition used in the research was according to the ‘BS EN ISO 4288:1998’ standard [61]. The surface profile of a deposited track is shown in Fig. 8.9.

After the deposition process, the samples were prepared for microstructural characterization. The samples were cut in the perpendicular to the direction of scan to reveal the cross section. The substrate material was also cut to reveal the cross section using the Mecatome T300. Both the surface and the cross section of the

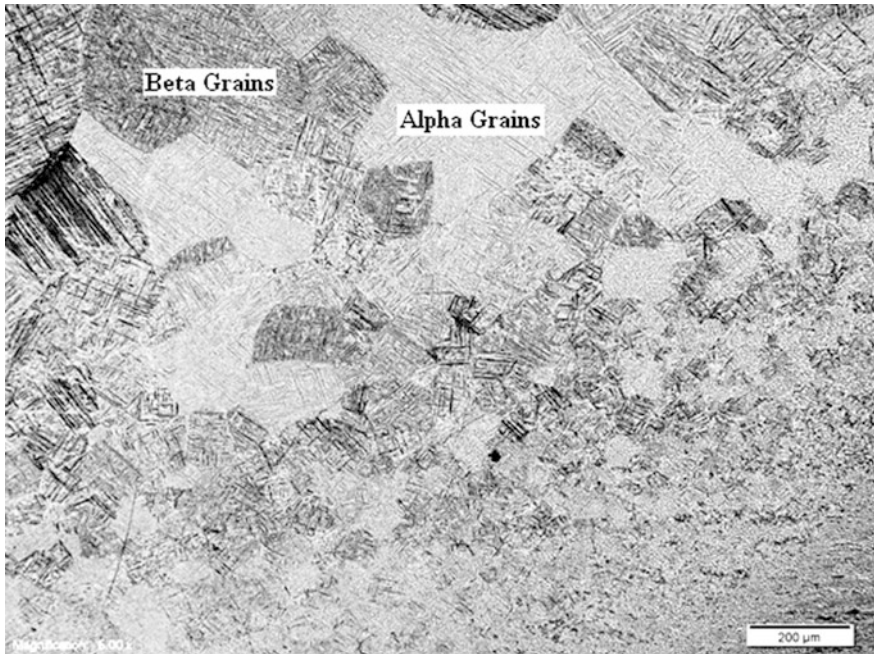


Fig. 8.10 An etched Ti6Al4V laser deposited sample

substrate were mounted in polyfast resin, using the Lecco PR 25 hot mounting press. The metallographic sample preparation was done, according to the standard metallurgical preparation of Titanium and its alloy, the ASTM E3-11 standard [26]. The polished samples were etched with Kroll's reagent. The Kroll's reagent consists of 100 ml of water with 1-3 ml of hydrofluoric acid and 2-6 ml of nitric acid. This etchant colours the beta phase dark brown. Figure 10 shows an etched sample of Ti6Al4V showing the alpha (brighter) and beta (darker) phases.

The microstructural studies were carried out under Olympus BX51 M Optical Microscopy (OP) equipped with an Olympus DP25 digital camera. The microscope with magnifications from $50\times$ to $1000\times$ was connected to the computer system equipped with Stream software for image analysis. TESCAN Scanning Electron Microscopy (SEM) equipped with Oxford Energy Dispersion Spectrometry (EDS) was used, in order to take high magnification images of the samples.

The SEM has a resolution of 0.3 nm, magnification range from $5\times$ to $300,000\times$, and an accelerating voltage in the range of 0.3–30 kV and the working distance between 15 and 25 mm. The purpose of using the SEM was to provide high resolution and high magnification images of the samples, in order to investigate the metallographic changes in the samples, as a result of the changing processing parameters. The energy dispersion spectrometry (EDS) helped to give quantitative and qualitative elemental analyses of certain regions on the imaged sample to obtain the elemental composition and distribution in the regions of interest. An Ultima IV

X-ray diffractometer (XRD) was used to study the phases in the samples. The XRD analysis was performed using $\text{MoK}\alpha$ radiations at a power setting of 40 kV and 4 mA.

The mechanical testing that were performed on the samples is the microhardness profiling. The hardness is the measure of the resistance of the material to permanent indentation. The size of the resulting indentation is an indication of the hardness of the material. The microhardness profile was taken on the cross-section of all the samples using the Metkon microhardness tester. A load of 500 g was used at a dwelling time of 15 s, and the distance between the indentations was kept at 12 μm , according to ASTM E384-11e1 standard [62].

The wear-resistance test was performed using a universal material tester UMT 2CETR tribotester with ball-on-plate arrangement under dry condition (no lubrication). The ball is a Tungsten Carbide sphere with a diameter 10 mm, at a load of 25 N, stroke length of 2 mm, and a reciprocating frequency of 20 Hz and for 1200 s. The coefficient of friction was measured for all the samples and recorded. The wear test was performed, according to ASTM G133—05(2010) Standard [63]. The wear surface was analyzed using the optical microscope, SEM and stylus surface analyzer (Jenoptik). The wear volumes were determined from information obtained from the wear-track surface profile, using the stylus surface analyzer and the optical microscope (that is, the cross-section of a wear track). As the stylus was

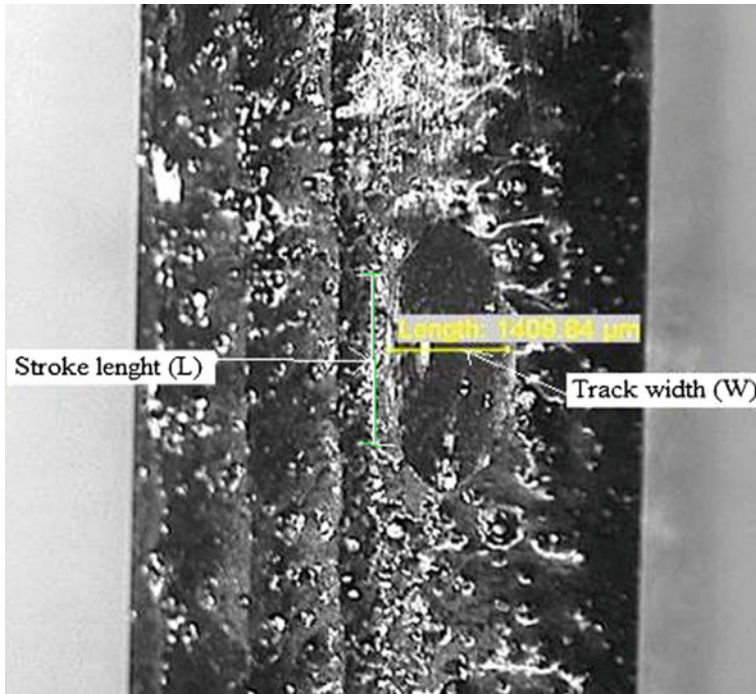


Fig. 8.11 Micrograph of a wear track showing the wear-track width and the stroke length

moved across the wear track, the vertical and horizontal positions of the stylus were recorded for the 2D wear profile of the track. An optical microscope was also used to measure the cross section, in order to ensure precision. Then the wear volume loss was obtained by using the formula proposed by Sharma et al. [64] in Eq. 8.1. An optical micrograph of a wear track is shown in Fig. 8.11.

$$V = L \left[r^2 \sin^{-1} \left(\frac{w}{2r} \right) - \frac{w}{2} \left(r^2 - \frac{w^2}{4} \right)^{1/2} \right] + \frac{\pi}{3} \left[2r^3 - 2r^2 \left(r^2 - \frac{w^2}{4} \right)^{1/2} - \frac{w^2}{4} \left(r^2 - \frac{w^2}{4} \right)^{1/2} \right]. \quad (8.1)$$

where v is the wear volume in mm^3 , r is the ball radius, w and L are the wear-track width and the stroke length, respectively. The wear volume was calculated by using Eq. 8.1.

8.3.4 Results and Discussion

The SEM micrograph of the Ti6Al4V powder and substrate are shown in Fig. 8.2. The SEM micrograph of the TiC powder is shown in Fig. 8.12. The TiC powder particle size analysis is shown in Fig. 8.13a it is in the range below $60 \mu\text{m}$ and it is

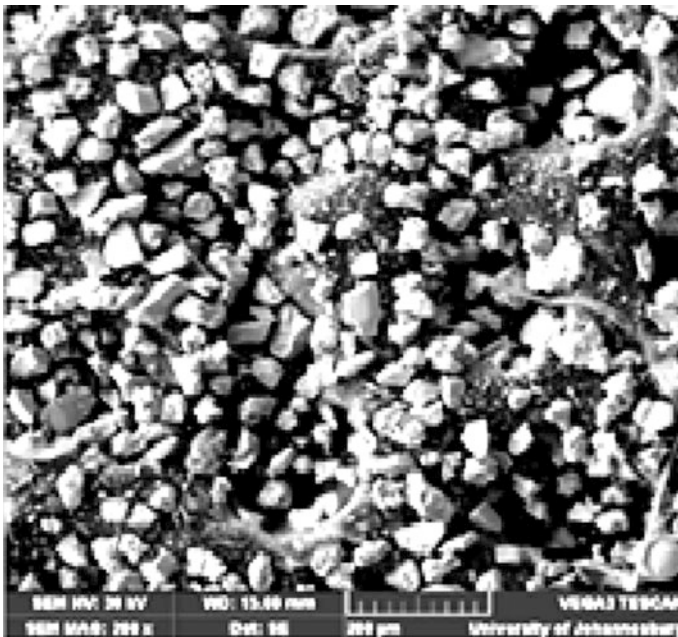


Fig. 8.12 TiC powder

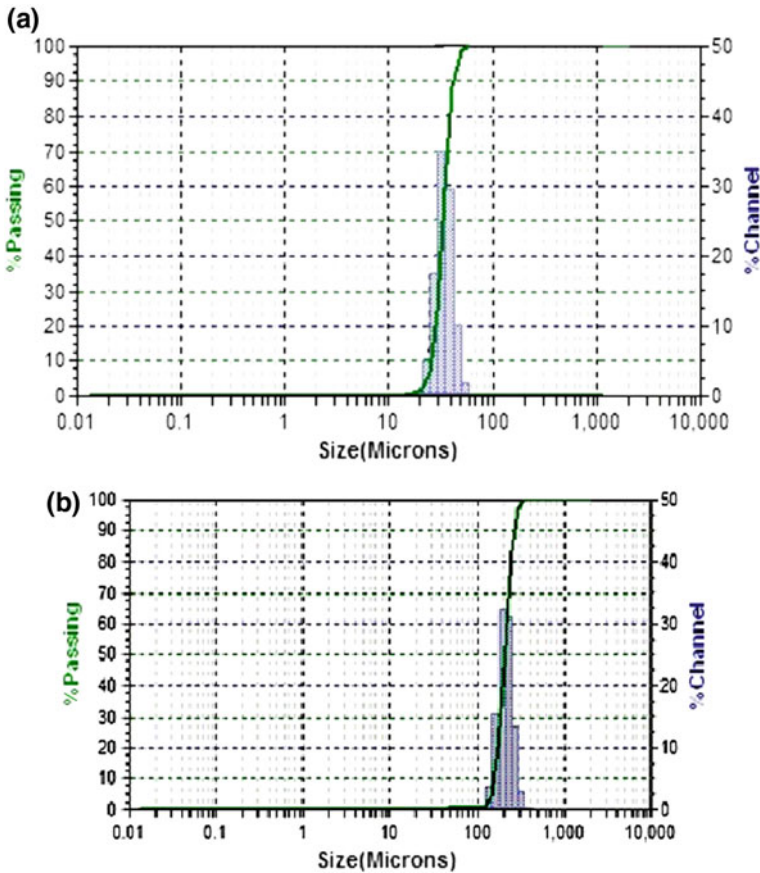


Fig. 8.13 Particle size analysis of **a** TiC powder **b** Ti6Al4V powder

characterized by irregular shape morphology that is typical of ball milled powder. The Ti6Al4V powder size is in the range of 150–350 μm . The particle size analysis is shown in Fig. 8.13b. The micrograph of the composite of the sample at a laser power of 1.6 kW is shown in Fig. 8.3. The macrograph of the deposited composite is shown in Fig. 8.14. The microstructure consists of Unmelted Carbides (UMC), dendritic TiC and re-solidified carbide. At low laser power, the microstructure consists of mainly unmelted TiC and some dendritic TiC. The melt pool created by the laser on the substrate makes the substrate to conduct the heat away as quickly as possible because the substrate is at room temperature; this causes the directional solidification as observed in the LMD process.

The grains of the substrate near the melt pool gain heat from the melt pool and results in grain growth, this forms a globular grains. The size of the globular grains reduced across the depth of the substrate because the grains far away from the melt pool gain less heat and hence less grain growth that results in smaller grain growth,

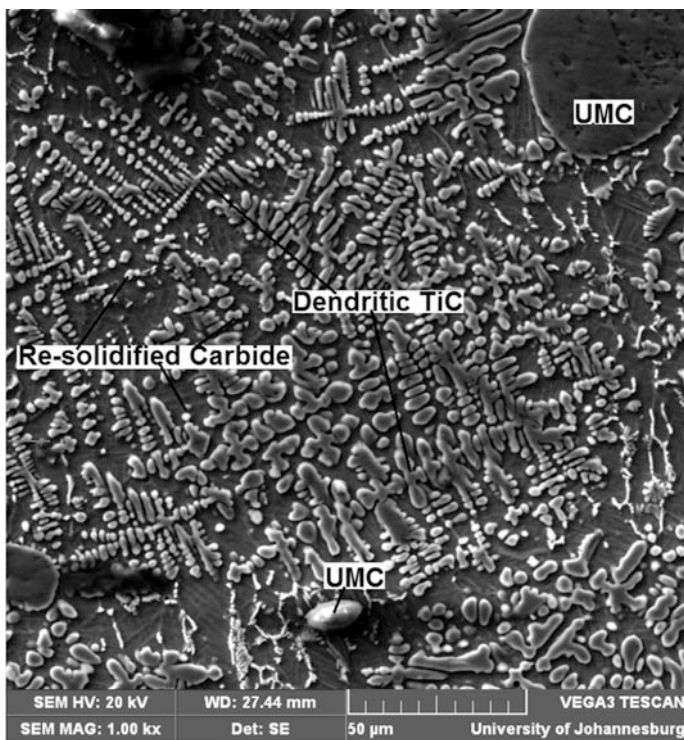


Fig. 8.14 SEM micrograph of sample at laser power of 1.5 kW

hence smaller globular grains. The rest of the structure grows epitaxially on the globular grains. The ratio of the unmelted carbide reduces as the laser power was increased. At a laser power of 2 kW the unmelted carbide disappeared and the microstructure consists of majorly dendritic TiC and re-solidified or secondary carbide as shown in Fig. 8.15. As the laser power was further increased, the microstructure consists mainly of dendritic TiC and re-solidified carbide with the dendritic arm reducing as the laser power was increased. The micrograph of sample produced at laser power of 3 kW is shown in Fig. 8.16. Comparing Figs. 8.15 and 8.16, it can be seen that the dendritic arm of the dendritic TiC arm in Fig. 8.15 is very long and the dendritic arm has almost disappear in Fig. 8.16 at very high laser power. The micrograph in Fig. 8.16 consists of mainly re-solidified carbide or secondary carbide.

At lower laser power, the deposited powders are not fully melted because the available laser power was not sufficient to fully melt the deposited powder. This is why there are unmelted carbides TiC found at low laser power as is seen in Fig. 8.14. As the laser power was increased more and more of the powders are melted. At moderately high laser power that is just sufficient to fully melt the deposited powders, the solidification is rapid and dendritic TiC are seen majorly in

Fig. 8.15 SEM micrograph of sample produced at laser power of 2 kW **a** at low magnification **b** high magnification

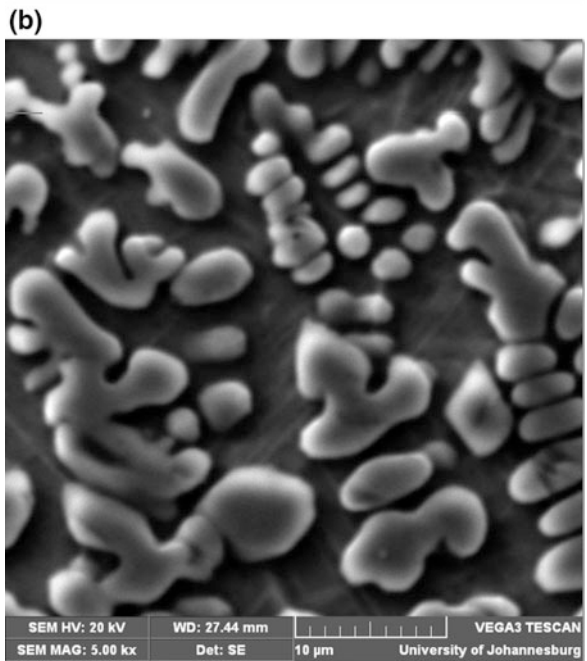
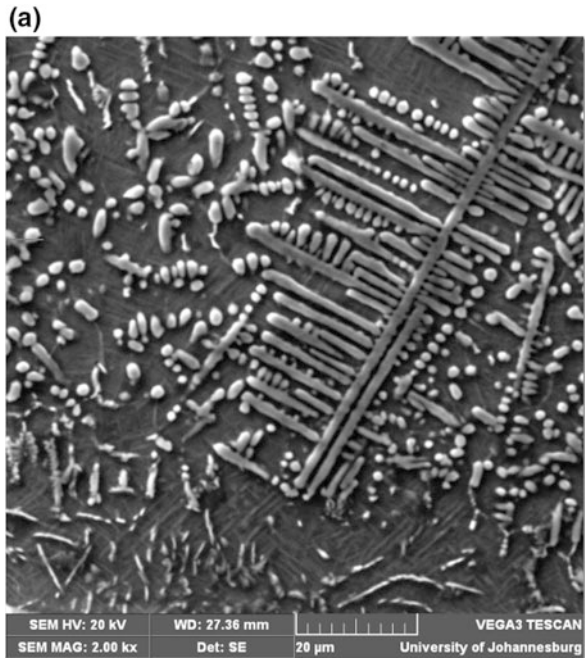


Fig. 8.16 SEM micrograph at laser power of 3 kW at **a** low magnification and **b** higher magnification

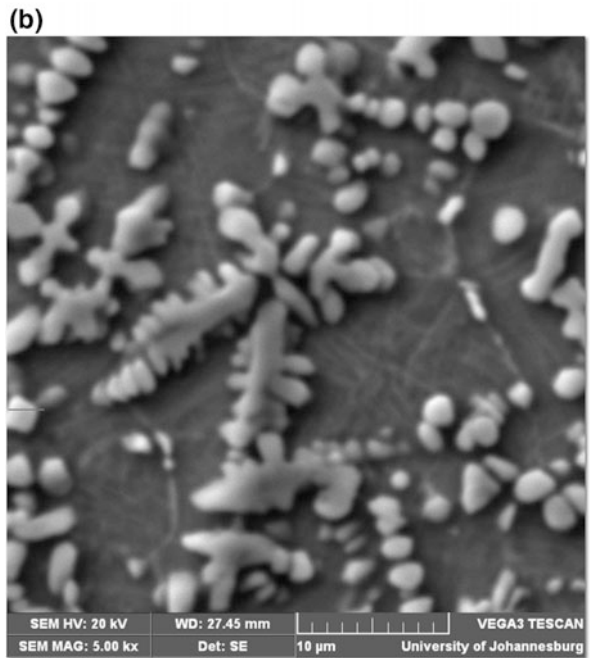
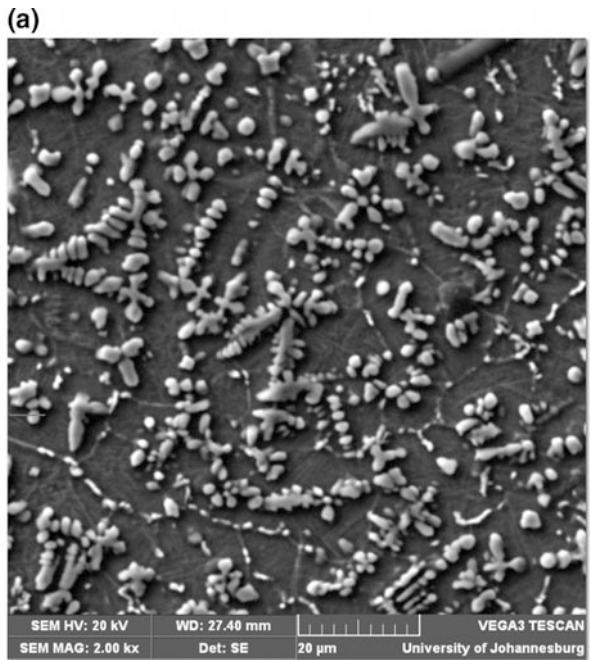


Table 8.6 Table of results

S/N	Laser power (kW)	Microhardness (HV)	Wear volume (mm ³)
0	Substrate	300.02	0.178
1	1	380.23	0.043
2	1.5	364.54	0.048
3	2.0	358.67	0.054
4	2.5	345.78	0.062
5	3.0	320.27	0.071

the microstructure with long dendritic arms. As the laser power was further increased beyond what was sufficient to fully melt the powders, this generated larger melt pool and the solidification is less rapid making more of re-solidified carbide or secondary carbide are more prominent at higher laser power. Less of dendritic carbides are seen and with low dendritic arms.

The microstructure has a direct relationship with properties. The results of the microhardness and the wear volume are presented in Table 8.6. The microhardness is found to reduce as the laser power is increased. The reason for this is not farfetched from the microstructural examination as was earlier explained.

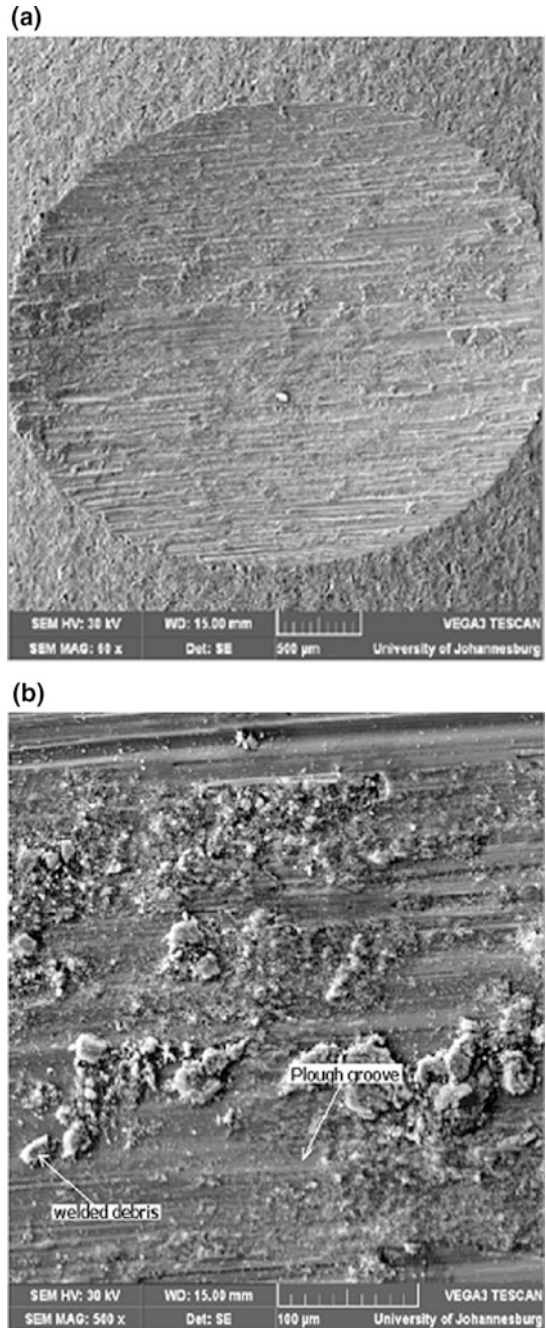
The very high microhardness values observed at low laser power could be attributed to the higher quantity of the unmelted carbide that are seen in the microstructure due to improper melting of the powders thereby retaining some of the TiC carbide particles that are merely melted on the surface. As the laser power was further increased, the dendritic TiC grew bigger with longer dendritic arms which are also very hard. As the laser power was further increased, the dendritic TiC decreased and the secondary TiC further increased. The secondary TiC is softer there by given rise to a lower microhardness values.

The dry sliding wear test result is presented in Table 8.6. The wear volume loss is found to increase as the laser power was increased. The analysis of the worn surfaces confirmed that the unmelted carbide found in the microstructure was responsible for the lower wear volume. The wear on the substrate is characterized by the ploughing grooves as shown in Fig. 8.17. The loose debris seen on the wear track are the work hardened Ti6Al4V particles that are produced during the rubbing action of the surface of the Ti6Al4V and the counter body. The wear mechanism is a combination of abrasion, adhesion and plastic deformation [25]. As the rubbing action continues, the frictional force between the two increased causing tearing of some of the surface material to chip off and with chips adhering to the surfaces.

The adhesion of the chip in the midst of rubbing action changed the wear mechanism from two body to three body wear mechanism causing generation of high temperature. The chips become work hardened and tear deep into the surface causing the ploughing ridges as seen in the Fig. 8.17. The wear tracks of the sample at a laser power of 3 kW and at 1 kW are shown in Fig. 8.18 and 8.19 respectively.

The unmelted carbide in the sample at a laser power of 1 kW helped to improve the wear resistance. The unmelted carbide got ground and reduced to fine powder that form protective coatings on the rubbing surfaces thereby reducing the wear

Fig. 8.17 The SEM micrograph of the wear track of the substrate at **a** low magnification and **b** higher magnification [25]



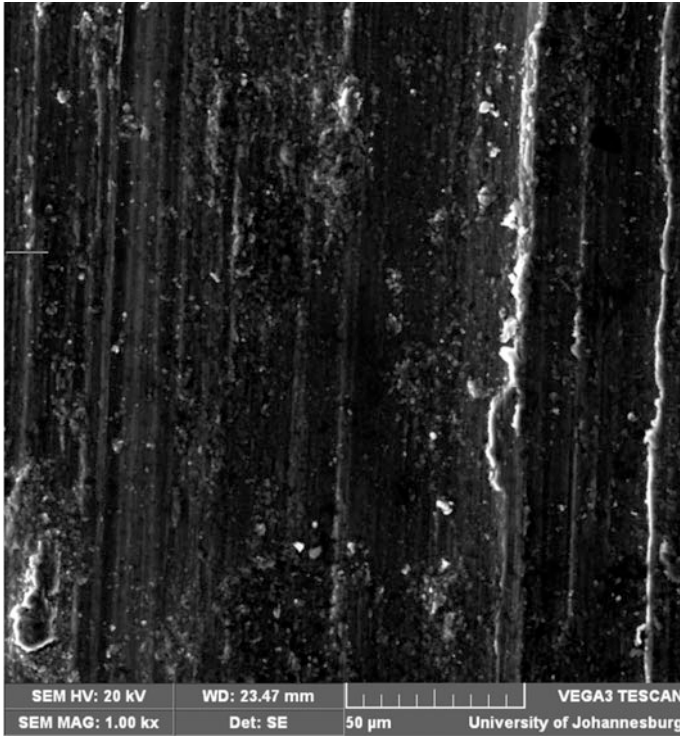


Fig. 8.18 SEM micrograph of sample at a laser power of 3 kW

action. The sample at a laser power of 3 kW showed wear track that is more aggravated because of the absence of the unmelted carbide particles. The wear track is much better than that of the substrate because the re-solidified carbides also help to improve the wear action.

8.4 Summary

The laser metal deposition of Ti6Al4V and Ti6Al4V/TiC composite has been presented in this chapter. The laser metal deposition process was seen to be very sensitive to processing parameters and it has been presented. Understanding the influence the processing parameter on the evolving properties will go a long way in controlling the properties of laser metal deposited materials. Also, an effective control system can be developed for the system to effectively control the properties of the deposited parts.

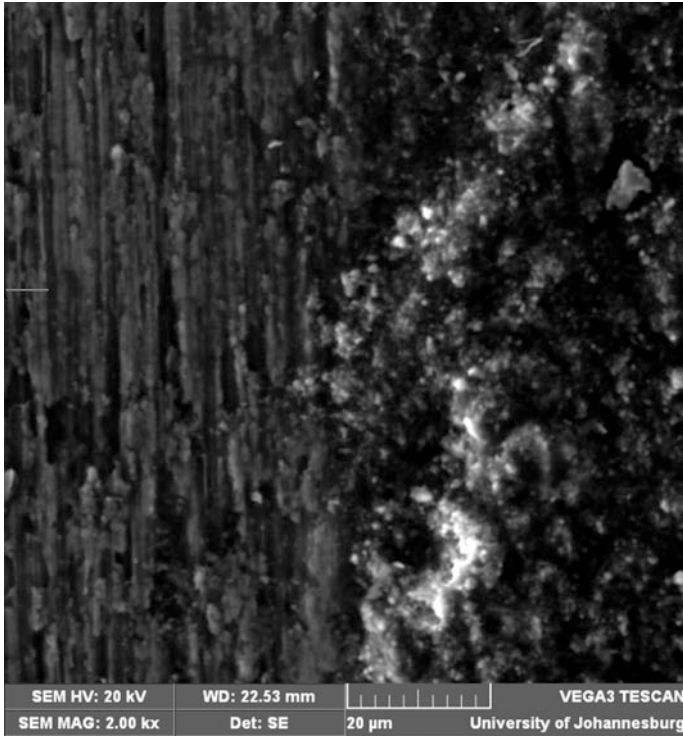


Fig. 8.19 SEM micrograph of the wear tracks of samples at a laser power of 1 kW

Acknowledgements This work was supported by University of Johannesburg research council, University of Ilorin and the L'OREAL-UNESCO for Women in Science.

References

1. Cui XH, Mao YS, Wei MX, Wang SQ (2012) Wear Characteristics of Ti-6Al-4V alloy at 20–400 °C. *Tribol Trans* 55(2):185–190
2. Askeland DR, Fulay PP, Wright WJ (2011) *The science and engineering of materials*, 6th edn. Global Engineering, Canada
3. Ezugwu EO, Wang ZM (1997) Titanium alloys and their machinability a review. *J Mater Process Technol* 68:262–274
4. Machado AR, Wallbank J (1990) Machining of titanium and its alloys a review. *Proc Inst Mech Eng Part B J Eng Manuf* 204:53–60
5. Yang X, Liu CR (1999) Machining titanium and its alloys. *Mach Sci Technol* 3(1):107–139
6. Mahamood RM, Akinlabi ET, Shukla M, Pityana S (2014) Revolutionary additive manufacturing: an overview. *Lasers Eng* 27:161–178
7. Scott J, Gupta N, Wember C, Newsom S, Wohlers T, Caffrey T (2012) Additive manufacturing: status and opportunities. Science and Technology Policy Institute.

- Available from https://www.ida.org/stpi/occasionalpapers/papers/AM3D_33012_Final.pdf. Accessed on 11 Jan 2017
8. Mahamood RM, Akinlabi ET, Shukla M, Pityana S (2013) The role of transverse speed on deposition height and material efficiency in laser deposited titanium alloy. In: 2013 international multi-conference of engineering and computer science (IMECS 2013), March 2013, pp 876–881
 9. Mahamood RM, Akinlabi ET, Shukla M, Pityana S (2012) Effect of laser power on material efficiency, layer height and width of laser metal deposited Ti6Al4V. In: world congress of engineering and computer science, San Francisco 2012, 24–26 October 2012, pp 1433–1438
 10. Mahamood RM, Akinlabi ET, Shukla M, Pityana S (2013) Material efficiency of laser metal deposited Ti6Al4V: effect of laser power. *Eng Lett* 21(1):EL_21_1_03. Available online at http://www.engineeringletters.com/issues_v21/issue_1/EL_21_1_03.pdf
 11. Akinlabi ET, Mahamood RM, Shukla M, Pityana S (2012) Effect of scanning speed on material efficiency of laser metal deposited Ti6Al4V. *World Academy of Science and Technology*, Paris 2012, vol 6, pp 58–62
 12. Mahamood RM, Akinlabi ET, Shukla M, Pityana S (2013) Laser metal deposition of Ti6Al4V: a study on the effect of laser power on microstructure and microhardness. In: International multi-conference of engineering and computer science (IMECS 2013), March 2013, pp 994–999
 13. Pityana S, Mahamood RM, Akinlabi ET, Shukla M (2013) Effect of gas flow rate and powder flow rate on properties of laser metal deposited Ti6Al4V. In: 2013 international multi-conference of engineering and computer science (IMECS 2013), March 2013, pp 848–851
 14. Mahamood RM, Akinlabi ET, Shukla M, Pityana S (2013) Characterizing the effect of processing parameters on the porosity properties of laser deposited titanium alloy. In: International multi-conference of engineering and computer science (IMECS 2014)
 15. Mahamood RM, Akinlabi ET (2016) Process parameters optimization for material deposition efficiency in laser metal deposited titanium alloy. *Lasers Manuf Mater Proces* 3(1):9–21. doi:10.1007/s40516-015-0020-5
 16. Mahamood RM, Akinlabi ET, Akinlabi SA (2014) Laser power and scanning speed influence on the mechanical property of laser metal deposited titanium-alloy. *Lasers Manuf Mater Proces* 2(1):43–55
 17. Mahamood RM, Akinlabi ET, Shukla M, Pityana S (2013) Characterizing the effect of laser power density on microstructure, microhardness and surface finish of laser deposited titanium alloy. *J Manuf Sci Eng* 135(6):064502–064502-4. doi:10.1115/1.4025737
 18. ErmachenkoAG, Lutfullin RY, Mulyukov RR (2011) Advanced technologies of processing titanium alloys and their applications in industry. *Rev Adv Mater Sci* 29:68–82
 19. Richter E, Orban KH, Nowotny S (2004) Laser cladding of the Titanium alloy Ti6242 to restore damaged blades. In: Proceedings of 23rd international congress on applications of lasers and electro-optics
 20. Mahamood RM, Akinlabi ET (2016) Achieving mass customization through additive manufacturing. In: Schlick C, Trzcieliński S (eds) *Advances in ergonomics of manufacturing: managing the enterprise of the future*. Advances in Intelligent Systems and Computing, vol 490. Springer, Switzerland
 21. Allen J (2006) An investigation into the comparative costs of additive manufacture vs. machine from solid for aero engine parts. In: *Cost effective manufacture via net-shape processing*, meeting proceedings RTO-MP-AVT-139, Paper 17, 2006, pp 1–10
 22. Graf B, Gumenyuk A, Rethmeier M (2012) Laser metal deposition as repair technology for stainless steel and Titanium alloys. *Phys Proc* 39:376–381
 23. Pinkerton AJ, Wang W, Li L (2008) Component repair using laser direct metal deposition. *J Eng Manuf* 222:827–836
 24. Mahamood RM, Akinlabi ET (2017) Scanning speed influence on the microstructure and micro hardness properties of titanium alloy produced by laser metal deposition process. *Materials today: Proceedings* 4(4):5206–5214

25. Mahamood RM, Akinlabi ET, Shukla M, Pityana S (2013) Scanning velocity influence on microstructure, microhardness and wear resistance performance on laser deposited Ti6Al4V/TiC composite. *Mater Des* 50:656–666
26. E3 – 11 (2011) Standard guide for preparation of metallographic specimens. ASTM international Book of Standards, vol 03.01
27. Ermachenko AG, Lutfullin RY, Mulyukov RR (2011) Advanced technologies of processing titanium alloys and their applications in industry. *Rev Adv Mater Sci* 29:68–82
28. Donachi MJ (2000) Titanium—a technical guide, 2nd edn. ASM International, Metals Park, OH
29. Lütjering G, Williams JC (2003) Titanium. Springer, Berlin, Germany
30. Arrazola PJ, Garay A, Iriarte LM, Armendia M, Marya S, Le Maître F (2009) Machinability of Titanium alloys (Ti6Al4V and Ti555.3). *J Mater Process Technol* 209(5):2223–2230
31. Zhang S, Wu WT, Wang MC, Man HC (2001) In situ synthesis and wear performance of TiC particle reinforced composite coating on alloy Ti6Al4V. *Surf Coat Technol* 138(1):95–100
32. Straffelini G, Andriani A, Tesi B, Molinari A, Galvanetto E (2004) Lubricated rolling sliding behaviour of ion nitride and untreated Ti.6Al.4V. *Wear* 256(3–4):346–352
33. Miyoshi K (2001) Solid lubrication fundamentals and applications. Marcel Dekker, New York
34. Balla VK, Bhat A, Bose S, Bandyopadhyay A (2012) Laser processed TiN reinforced Ti6Al4V composite coatings. *J Mech Behav Biomed Mater* 6:9–20
35. Popoola API, Ochonogor OF, Abdulwahab M, Pityana S, Meacock C (2012) Microhardness and wear behaviour of surface modified Ti6Al4V/Zr-TiC metal matrix composite for advanced material. *J Optoelectr Adv Mater* 14(11–12):991–997
36. Kubiak KJ, Pawlak W, Wendler BG, Mathia TG (2013) Wear resistant multilayer nanocomposite WC1-x/C coating on Ti-6Al-4V titanium alloy. In: 40th Leeds-Lyon symposium on tribology and tribochemistry Forum, September 4–6 2013, Lyon, France
37. Popoola API, Ochonogor OF, Abdulwahab M (2013) Corrosion and hardness characteristics of laser surface modified Ti6Al4V/Zr+ TiC and Ti6Al4V/Ti+ TiC composites. *Int J Electrochem Sci* 8:2449–2458
38. Bejjani R, Balazinski M, Shi B, Attia H, Kishawy H (2011) Machinability and chip formation of titanium metal matrix composites. *Int J Adv Manuf Syst* 13(1):75–90
39. Poletti C, Merstallinger A, Schubert T, Marketz W, Degischer HP (2004) Wear and friction coefficient of particle reinforced Ti-alloys. *Mater Sci Eng Technol* 35(10–11):741–749
40. Abkowitz S, Abkowitz SM, Fisher H, Schwartz PJ (2004) CermeTi® discontinuously reinforced Ti-matrix composites: manufacturing, properties, and applications. *J Min Met Mater Soc* 56(5):37–41
41. Wang F, Mei J, Jiang H, Wu X (2007) Laser fabrication of Ti6Al4V/TiC composites using simultaneous powder and wire feed. *Mater Sci Eng A* 445–446:461–466
42. Kim YJ, Chung H, Kang SJL (2002) Processing and mechanical properties of Ti–6Al–4V/TiC in situ composite fabricated by gas–solid reaction. *Mater Sci Eng A* 333(1–2):343–350
43. Cui ZD, Zhu SL, Man HC, Yang XJ (2005) Microstructure and wear performance of gradient Ti/TiN metal matrix composite coating synthesized using a gas nitriding technology. *Surf Coat Technol* 190(2–3):309–313
44. Joshi PB, Marathe GR, Murti NSS, Kaushik VK, Ramakrishnan P (2002) Reactive synthesis of titanium matrix composite powders. *Mater Lett* 56(3):322–328
45. Selamat MS, Watson LM, Baker TN (2003) XRD and XPS studies on surface MMC layer of SiC reinforced Ti–6Al–4V alloy. *J Mater Process Technol* 142(3):725–737
46. Lapin J, Ondruš L, Bajana O (2003) Effect of Al₂O₃ particles on mechanical properties of directionally solidified intermetallic Ti–46Al–2W–0.5Si alloy. *Mater Sci Eng A* 360(1–2):85–95
47. de Castro V, Leguey T, Muñoz A, Monge MA, Pareja R (2006) Microstructure and tensile properties of Y₂O₃-dispersed Titanium produced by arc melting. *Mater Sci Eng A* 422(1–2):189–197
48. Zhanga E, Zenga S, Wang B (2002) Preparation and microstructure of in situ particle reinforced Titanium matrix alloy. *J Mater Process Technol* 125–126:103–109

49. Lloyd DJ (1990) Particulate reinforced composites produced by molten mixing. In: Das SK, Ballard CP, Marikar F (eds) High performance composites for the 1990s. TMS-New Jersey, pp 33–46
50. Eskandarany MS (2000) Structure and properties of nanocrystalline TiC full density bulk alloy consolidated from mechanically reacted powders. *J Alloy Compd* 305(1–2):225–238
51. Miracle DB (2005) Metal matrix composites—from science to technological significance. *Comp Sci Technol* 65(15–16):2526–2540
52. Kennedy R, Karantzalis AE, Wyatt SM (1999) The microstructure and mechanical properties of TiC and TiB₂-reinforced cast metal matrix composites. *J Mater Sci* 34(5):933–940
53. Loretto MH, Konitzer DG (1990) The effect of matrix reinforcement reaction on fracture in Ti-6Al-4V-base composites. *Metallur Trans A* 21(6):1579–1587
54. Nalla RK, Ritchi RO, Boyce BL, Campbell JP, Peters JO (2002) Influence of microstructure on high-cycle fatigue of Ti-6Al-4V: bimodal vs. lamellar structures. *Metallur Mater Trans A* 33(3):899–918
55. Singermann SA, Jackson JJ (1996) Titanium metal matrix composite for aerospace applications. In: Proceedings of eighth international symposium on superalloys, pp 579–586
56. Mahamood RM, Akinlabi ET (2015) Effect of processing parameters on wear resistance property of laser material deposited titanium-alloy composite. *J Optoelectr Adv Mater (JOAM)* 17(9–10):1348–1360
57. Mahamood RM, Akinlabi ET (2015) Effect of laser power and powder flow rate on the wear resistance behaviour of laser metal deposited TiC/Ti6Al4V composites. *Mater Today Proc* 2(4–5):2679–2686
58. Mahamood RM, Akinlabi ET, Shukla M, Pityana S (2014) Characterization of laser deposited Ti6Al4V/TiC composite. *Lasers Eng* 29(3–4):197–213
59. Obielodan J, Stucker B (2013) Characterization of LENS-fabricated Ti6Al4V and Ti6Al4V/TiC dual-material transition joints. *Int J Adv Manuf Technol* 66(9–12):2053–2061
60. Ochonogor OF, Meacock C, Abdulwahab M, Pityana S, Popoola API (2012) Effects of Ti and TiC ceramic powder on laser clad Ti-6Al-4V in situ intermetallic composite. *Appl Surf Sci* 263:591–596
61. BS EN ISO 4288 (1998) Geometric product specification (GPS). Surface texture. Profile method: rules and procedures for the assessment of surface texture, BSI
62. ASTM E384 - 11e1 (2011) Standard test method for Knoop and Vickers hardness of materials. ASTM International Book of Standards, vol 03.01
63. ASTM G133 - 05(2010) Standard test method for linearly reciprocating ball-on-flat sliding wear. ASTM International Book of Standards, vol 03.02
64. Sharma S, Sangal S, Mondal K (2013) On the optical microscopic method for the determination of ball-on-flat surface linearly reciprocating sliding wear volume. *Wear* 300(1–2):82–89